Focal adhesion kinase is required for neural crest cell morphogenesis during mouse cardiovascular development

Ainara Vallejo-Illarramendi, Keling Zang, and Louis F. Reichardt

Department of Physiology, UCSF, San Francisco, California, USA.

Neural crest cells (NCCs) participate in the remodeling of the cardiac outflow tract and pharyngeal arch arteries during cardiovascular development. Focal adhesion kinase (FAK) mediates signal transduction by integrin and growth factor receptors, each of which is important for normal cardiovascular development. To investigate the role of FAK in NCC morphogenesis, we deleted it in murine NCCs using *Wnt1cre*, yielding craniofacial and cardiovascular malformations resembling those observed in individuals with DiGeorge syndrome. In these mice, we observed normal cardiac NCC migration but reduced differentiation into smooth muscle within the aortic arch arteries and impaired cardiac outflow tract rotation, which resulted in a dextroposed aortic root. Moreover, within the conotruncal cushions, Fak-deficient NCCs formed a less organized mesenchyme, with reduced expression of perlecan and semaphorin 3C, and exhibited disorganized F-actin stress fibers within the aorticopulmonary septum. Additionally, absence of Fak resulted in reduced in vivo phosphorylation of Crkl and Erk1/2, components of a signaling pathway essential for NCC development. Consistent with this, both TGF-β and FGF induced FAK and Crkl phosphorylation in control but not Fak-deficient NCCs in vitro. Our results indicate that FAK plays an essential role in cardiac outflow tract development by promoting the activation of molecules such as Crkl and Erk1/2.

Introduction

Malformations of the cardiac outflow tract and aortic arch arteries are relatively common congenital defects in humans, and they result from a mixture of environment and genetic interactions, involving different cell types that include neural crest cells (NCCs). NCCs are essential for cardiovascular development, as they participate in septation of the cardiac outflow tract and remodeling of the pharyngeal arch arteries (1, 2). Cardiac NCCs migrate from the dorsal neural tube through the pharyngeal arches in response to poorly understood signals (3). In the pharyngeal arch arteries, cardiac NCCs differentiate into smooth muscle cells. Finally, cardiac NCCs migrate into the cardiac outflow tract, in which they contribute to the aorticopulmonary septation complex that divides the outflow tract into the aorta and pulmonary trunk (4). Abnormalities of these structures are involved in many clinically relevant congenital cardiac defects, such as in DiGeorge (also known as del22q11) syndrome, but the cellular and molecular defects in cardiac NCCs that are responsible for these abnormalities are incompletely understood (2). The genetic bases of DiGeorge syndrome are heterozygous deletions within human chromosome 22q11, involving genes such as T-box 1 (*Tbx1*) and v-crk sarcoma virus CT10 oncogene homolog (avian)-like (*Crkl*) that are positioned within the classical recurrent deletion. Cardiovascular defects observed in this syndrome, such as aortic arch interruption, persistent truncus arteriosus, and ventricular septal defects, are also observed in animal models with defects in NCC migration or differentiation or that are lacking Tbx1 or Crkl (5–7).

Focal adhesion kinase (FAK) is a cytoplasmic tyrosine kinase activated by integrin and growth factor signaling that has been implicated in numerous cellular processes, including cell migration, differentiation, survival and proliferation (8). Analysis of FAK in vivo is complicated by early embryonic lethality of mutant embryos (9). FAK regulates PI3 kinase, PLC-γ1, Erk, Rho, Arf, and other signaling molecules. FAK is activated by FGFs and other growth factors implicated in cardiovascular development, including PDGF and TGF-β (10, 11). Through Crk-associated substrate (p130 Cas), FAK also promotes Crk-mediated activation of several pathways, including Rac, Jun kinase, and Erk (8). Thus, FAK is a potential activator of the Crkl-regulated signaling pathways that appear to account for many phenotypes observed in DiGeorge syndrome (12, 13).

FAK is also activated by β_1 and β_3 integrin ligation and regulates cell motility through regulation of the cytoskeleton and integrin recycling (8). NCCs express multiple integrins that regulate the migratory behavior of NCCs in vivo and in vitro (14–16). Loss of β_1 integrin heterodimers in NCCs after initiation of migration using a Cre-recombinase under the control of the human tissue plasminogen activator promoter (Ht-PA-Cre) transgene results in aberrant development of the peripheral nervous system, but no cardiovascular abnormalities (17). However, earlier deletion of β_1 integrins from NCCs is reported to result in embryonic lethality at E12.5, with defects in cardiac NCC derivatives, although details have not been published (17). In addition, Pinch1, a scaffold protein associated with integrins and integrin-linked kinase, is required for normal development of cranial and cardiac NCC-derived structures, but the PINCH mutant phenotype differs significantly from that of DiGeorge syndrome (18).

Several of the growth factors implicated in cardiac development, including FGFs, TGF-β, and VEGF, regulate the inductive interactions between cardiac NCCs and the pharyngeal epithelium (19, 20). Data from murine models indicate that abnormal growth factor signaling leads to mispatterning of the outflow tract and pharyngeal arch arteries as well as intracardiac defects.

Conflict of interest: The authors have declared that no conflict of interest exists.

Nonstandard abbreviations used: FAK, focal adhesion kinase; NCC, neural crest cell; pAb, polyclonal Ab; qPCR, quantitative RT-PCR.

Citation for this article: *J. Clin. Invest.* **119**:2218–2230 (2009). doi:10.1172/JCI38194.

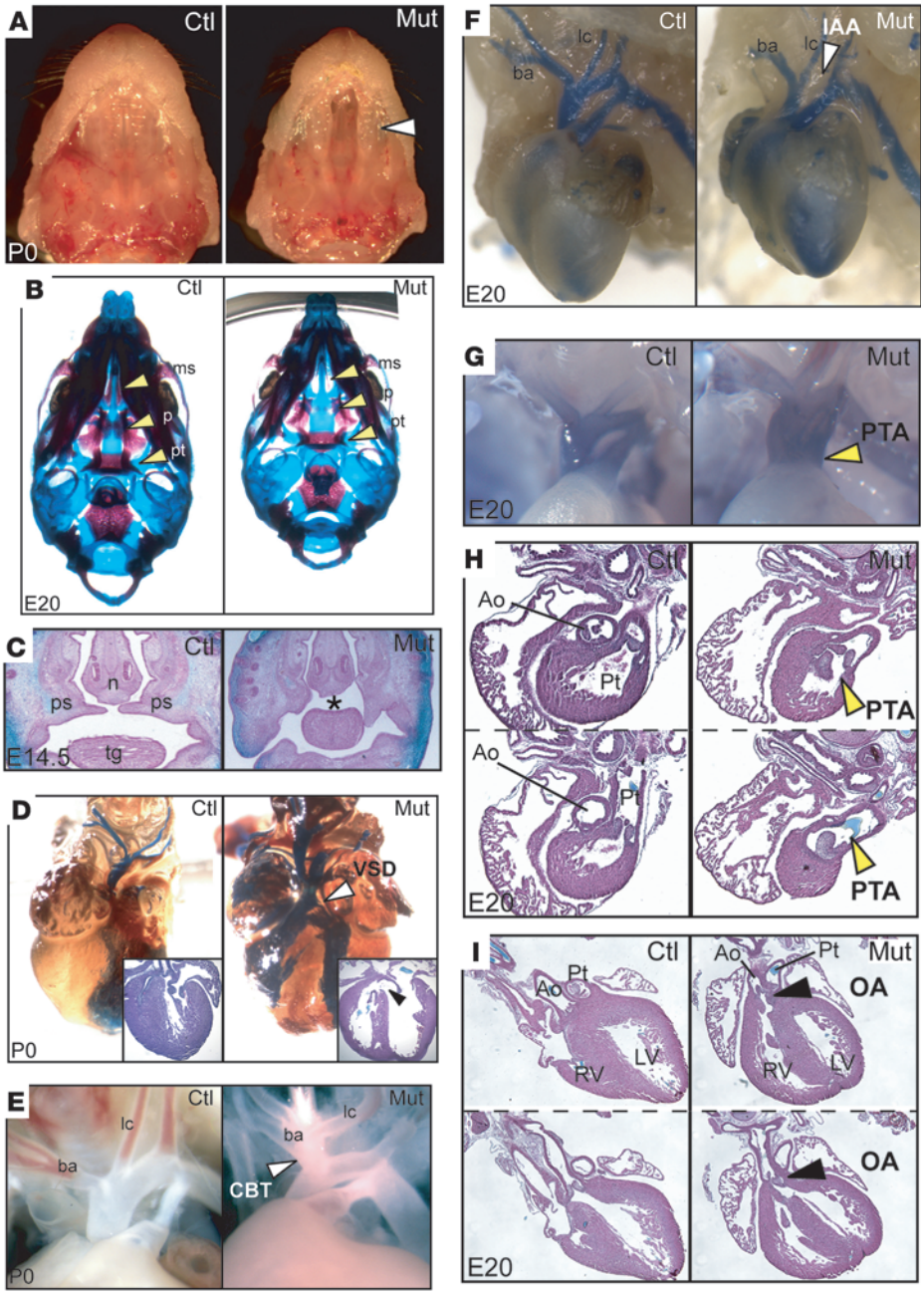

Figure 1
Cranial and cardiovascular defects in *Wnt1creFak*$^{flox/flox}$ mice. (**A**) *Wnt1cre-Fak*$^{flox/flox}$ mutants display a cleft palate (white arrowhead), with unfused palatal shelves. (**B**) Ventral view of E20 mutant and control skulls, stained with Alizarin Red (bone) and Alcian Blue (cartilage). Mutants show defective formation of the maxillary shelves (ms), palatine (p), and pterygoid process (pt) (yellow arrowheads). (**C**) E14.5 mutants show misplaced palatal shelves (ps) that failed to rotate or elevate (asterisk) and remained lateral to the tongue (tg). (**D**) Frontal view of P0 hearts injected with polymer casting material and cleared with Methyl salicylate, showing ventricular septal defects (VSD; arrowheads) in mutants. Insets show sections of these hearts stained with H&E. (**E** and **F**) Aortic arch artery phenotypes include a common brachiocephalic trunk (CBT; arrowhead in **E**) and interruption or coarctation of the aortic arch (IAA; arrowhead in **F**). Hearts in **F** were injected with blue polymer for better visualization of aortic arch patterning. (**G**–**I**) Outflow tract abnormalities in mutants include persistent truncus arteriosus (PTA) in **G** and **H** (yellow arrowheads) and overriding aorta (OA) in **I** (black arrowheads). (**H** and **I**) Paraffin-embedded cross (**H**) and frontal (**I**) serial sections from E20 hearts stained with H&E. Ao, aorta; ba, brachiocephalic artery; Ctl, control; lc, left carotid artery; Mut, *Wnt1creFak*$^{flox/flox}$ mutant; n, nasal septum; Pt, pulmonary trunk. Original magnification, ×4 (**A**, **B**, and **F**); ×10 (**C**–**E** and **G**–**I**).

Various growth factor deficiencies impair NCC differentiation into smooth muscle cells (21, 22), elevate NCC death (23–25), or reduce fibronectin expression (26).

Here, we describe a new model of congenital heart disease, resulting from ablation of *Fak* in NCCs using *Wnt1cre*. We show that FAK is essential for both morphogenetic patterning of the outflow tract and remodeling of aortic arch arteries, and we identify signaling pathways impaired in the mutant that are known to regulate these developmental events.

Results

Specific ablation of Fak from NCCs results in perinatal lethality. To investigate the function of FAK in cardiac NCCs in vivo, we crossed mice with a floxed allele of *Fak* (*Fak*$^{flox/flox}$) (27) with *Wnt1cre* mice to obtain specific *Fak* inactivation in NCCs. The *Wnt1cre* transgenic mouse line has been previously used in numerous studies for targeted gene deletion and lineage tracing of NCCs. The *Wnt1* promoter is first activated at E8.5 in the neural crest and results in extensive Cre-mediated recombination in neural crest derivatives (28). Efficient deletion of the *Fak* allele in conditional *Fak* mutants was confirmed using PCR and immunohistochemistry (Supplemental Figure 1, A and B; supplemental material available online with this article; doi:10.1172/JCI38194DS1). At E10.5, FAK expression in control tissue sections was high in the branchial arch mesenchyme, which is primarily derived from NCCs, and in overlying ectoderm. In contrast, in *Wnt1creFak*$^{flox/flox}$ mutants, FAK expression in the mesenchyme was almost completely abolished, although ectodermal expression persisted (Supplemental Figure

Table 1
Summary of phenotypes in late-term *Fak* mutants

Phenotype	Number	Penetrance
Cleft palate	14 of 21	67%
Ventricular septal defect	12 of 12	100%
Persistent truncus arteriosus	11 of 16	69%
Overriding aorta	5 of 20	25%
Interruption/coarctation of aortic arch	9 of 23	39%
Common brachiocephalic trunk	10 of 18	56%
Aortic arch defects[A]	11 of 18	61%

[A]Phenotypes including interruption/coarctation of aortic arch and/or common brachiocephalic trunk.

1C). The neural crest origin of branchial arch mesenchyme was assessed in E10.5 embryos via the additional inclusion of the Cre-regulated *Z/EG* reporter allele.

At E9.5 and E10.5, conditional *Fak* mutants did not exhibit any gross histological malformations. *Wnt1creFak*$^{flox/flox}$ mutants were recovered at the expected Mendelian ratios at all embryonic stages, but the majority of the conditional *Fak* mutants died between E20 and P2 (Supplemental Table 1). Only 1 of 54 mutants survived to P30. This animal was small and showed obvious motor abnormalities not characterized as part of this study.

Craniofacial and cardiovascular defects in Wnt1creFak$^{flox/flox}$ *mutants*. *Wnt1creFak*$^{flox/flox}$ embryos after E16.5 demonstrated multiple craniofacial and cardiovascular malformations, summarized in Table 1, none of which were observed in controls. NCCs in the branchial arches contribute to the bony and cartilaginous structures of the cranium (29), which we analyzed using Alcian Blue and Alizarin Red staining of E18.5–P0 animals (Figure 1). At these stages, most *Fak* mutants were smaller than control littermates. In *Wnt1creFak*$^{flox/flox}$ mutants, 67% of animals exhibited a cleft palate (Figure 1A). The secondary palate is composed of the maxillary and palatine bones that together form the palatal shelves. A ventral view of the mutant revealed that the pterygoid process was incompletely ossified and that the palatine and maxillary shelves had not formed properly and had failed to fuse (Figure 1B). Frontal sections of E14.5 embryos showed that, in contrast to control littermates, the palatal shelves of *Wnt1creFak*$^{flox/flox}$ embryos had neither rotated nor elevated (Figure 1C).

We analyzed cardiac structures by visual inspection and histological analysis, following vascular casting with polymer injected into the left ventricle. Our analysis demonstrated a spectrum of aortic arch patterning and cardiac outflow tract septation defects, summarized in Table 1. All mutants analyzed (12 of 12) exhibited a septation deficit between the left and right ventricles (Figure 1D). Aortic arch patterning defects (61%) included interruption or coarctation of the aortic arch (39%) and a common brachiocephalic trunk (58%), in which the left carotid artery branches from the brachiocephalic artery (Figure 1, E and F). When present, the interruption of the aortic arch was located between the left carotid and the left subclavian arteries (Figure 1F, arrowhead). Cardiac outflow tract abnormalities included persistent truncus arteriosus (69%) and overriding aorta (25%) (Figure 1, G–I). We also observed the presence of truncal valves, with variable cusp numbers associated with persistent truncus arteriosus (Figure 1H, showing 4 cusps). The observed cardiovascular and craniofacial malformations recapitulate common congenital defects that have been previously attributed to deficiencies in NCCs (30). These abnormalities are sufficient to explain the perinatal lethality of the conditional *Fak* mutants.

Effect of Fak deletion on NCC migration. To determine whether the aortic arch patterning and outflow tract septation defects observed in the conditional *Fak* mutants were due to defective NCC migration, we used the *R26R* (31) and the *Z/EG* (32) reporter alleles, in which Cre expression activates β-galactosidase and GFP expression, respectively. Using these, we followed NCCs as they migrated through the pharyngeal arch arteries, formed the aorticopulmonary septum, and differentiated into smooth muscle in the cardiac outflow tract. At E9.5 and E10.5, labeled NCCs were detected in the cranial, pharyngeal arch and trunk regions (Figure 2A). Distinct tracts of NCCs could be observed migrating through the somites and within axon fiber tracks. NCC migration appeared similar in conditional *Fak* mutants and control littermates.

To analyze NCC migration in more detail, we examined sagittal sections of E10.5 embryos. The paired streams of NCCs that migrate into the conotruncal cushions were present in similar numbers and distributions in control and mutant embryos (Figure 2A). At E12.5, we found obvious defects in the cardiac outflow tracts of conditional *Fak* mutants, including misalignment of the great arteries and presence of an abnormal aorticopulmonary communication (Figure 2B). However, we did not observe a major difference in the pattern or intensity of NCC staining at this time point. To rule out minor migratory defects, we quantified NCCs in the conotruncal cushions of E11.0 outflow tracts (Figure 2, C and D). There was no significant difference in NCC numbers between control and mutant embryos.

Overall, our data indicate that initial specification and migration of *Fak*-deficient NCCs is not altered in early cardiovascular development. It also suggests that there is no major alteration in *Fak*-deficient NCC proliferation or survival in the cardiac outflow tract at this stage. This result is further confirmed by analysis of cell proliferation and cell death in E9.5 embryos, in which we did not observe any obvious differences between conditional *Fak* mutant and control littermates (Supplemental Figure 2).

Effect of Fak deletion on NCC differentiation. To determine whether the cardiovascular defects observed in the *Wnt1creFak*$^{flox/flox}$ mutants were caused by defective differentiation of NCCs into smooth muscle, we analyzed the expression at E11.0 and E12.5 of SMA, a broadly used marker of smooth muscle differentiation. Failure of murine cardiac NCCs to differentiate into smooth muscle, as a result of deletion homologous to the human 22q11 region or impaired TGF-β signaling, has been shown to result in similar cardiovascular defects as the ones observed in conditional *Fak* mutants (21, 33). However, in the outflow tract region and, more specifically, in the aorticopulmonary septum, we did not observe altered expression of SMA in NCCs at either E11.0 or E12.5, even in mutant embryos with an obvious abnormal aorticopulmonary communication (Figure 3, A–F, and Supplemental Figure 3).

In addition, at these stages (E11.0 and E12.5), SMA also stains the myocardium as well as smooth muscle. Thus, we were able to analyze myocardialization of the outflow tract in these sections. Myocardialization begins at E12.5 in the mouse and occurs as a result of myocyte migration that contributes to the formation of the muscular portion of the outlet segments (34, 35). Several studies in mice with cardiac outflow tract malformations have reported defective myocardialization of this region (35–38). In the *Wnt1creFak*$^{flox/flox}$ mutant mice, however, we observed no obvious deficits

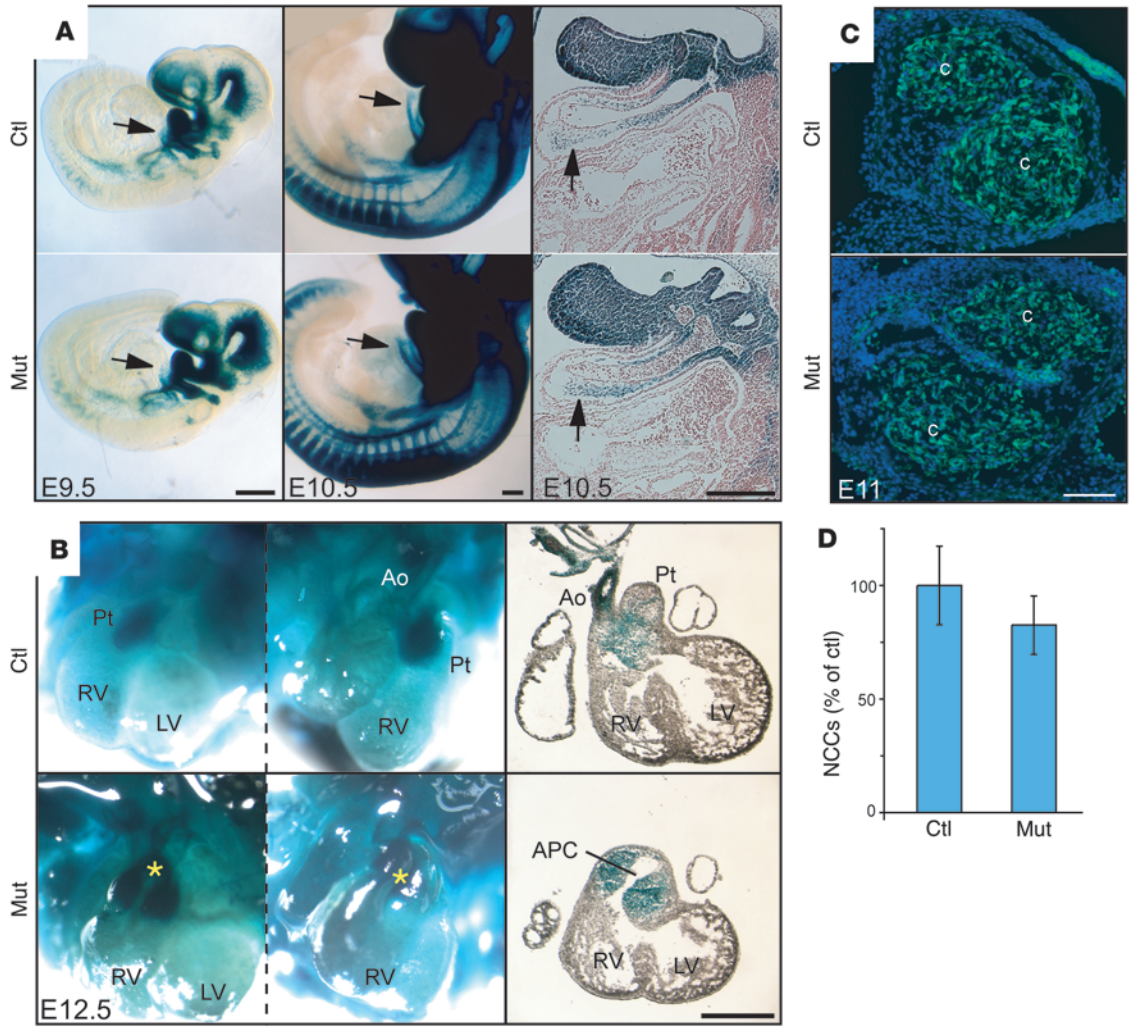

Figure 2

Normal neural crest migration in conditional *Fak* mutant embryos. (**A**) Whole mounts of E9.5 and E10.5 X-gal–stained embryos. The right column shows sagittal sections of E10.5 embryos stained with Fast Red. Arrows indicate colonization of the outflow tract by cardiac NCCs (blue). (**B**) Whole mounts of E12.5 X-gal–stained hearts. Asterisks show positions of the great arteries in mutant embryos, showing misalignment of the great arteries and abnormal aorticopulmonary communication (APC). The left column shows frontal views; the middle column shows right views; the right column shows frontal histological sections of the hearts. (**C**) Frontal cryostat sections of E11 embryos at distal outflow tract levels. Cardiac NCCs (green) are able to colonize the outflow tract of mutants and form conotruncal cushions (c). (**D**) No significant difference was found in the number of NCCs in E11 control and mutant outflow tracts. This analysis was performed using 10 serial sections, 30 μm apart, with locations matched between control and mutant littermates. A minimal conotruncal cushion area of 0.22 mm^2 was analyzed from each embryo. Data are expressed as mean ± SD. Scale bars: 250 μm (**A**); 500 μm (**B**); 100 μm (**C**).

in myocardialization of the outflow tracts at E12.5 (Figure 3, C–F, and Supplemental Figure 3).

In contrast, in the aortic arch region of the *Fak* mutants at E11.5, we observed decreases in SMA using Western blot (Figure 3H; $n = 3$) as well as immunohistochemistry, in which we detected localized defective differentiation of NCCs into smooth muscle in 60% of the *Fak* mutants (Figure 3, I–L; $n = 5$). All affected embryos showed impaired differentiation in the fourth aortic arch artery; some also showed decreased SMA expression in the third and/or sixth arch arteries (Figure 3, I and J). The deficits do not appear to be caused by increased NCC death, as determined by TUNEL (Figure 3, J and L). Interestingly, the percentage of embryos with defective smooth muscle differentiation in the aortic arch arteries is comparable to that of late-term mutants, showing alterations in aortic arch artery patterning (61%; Table 1). Moreover, at E12.5, we observed conditional *Fak* mutants with striking reductions of SMA in the aortic arch region between the left carotid and the left subclavian arteries (Figure 3, M–R). Notably, this is the same region in which interruption or coarctation of the aortic arch is observed at E20 (Figure 1F, arrowhead). Nonetheless, despite deficient smooth muscle differentiation in *Fak* mutants, we detected apparently normal NCC numbers and arterial tube formation in the region of the aortic arch arteries at E11.0 and E12.5 (Figure 3, I and J and O–T), with no detectable increase in cell death (Figure 3, P and U). Thus, reduced SMA staining in this region does not appear to be due to deficits in NCC migration or survival.

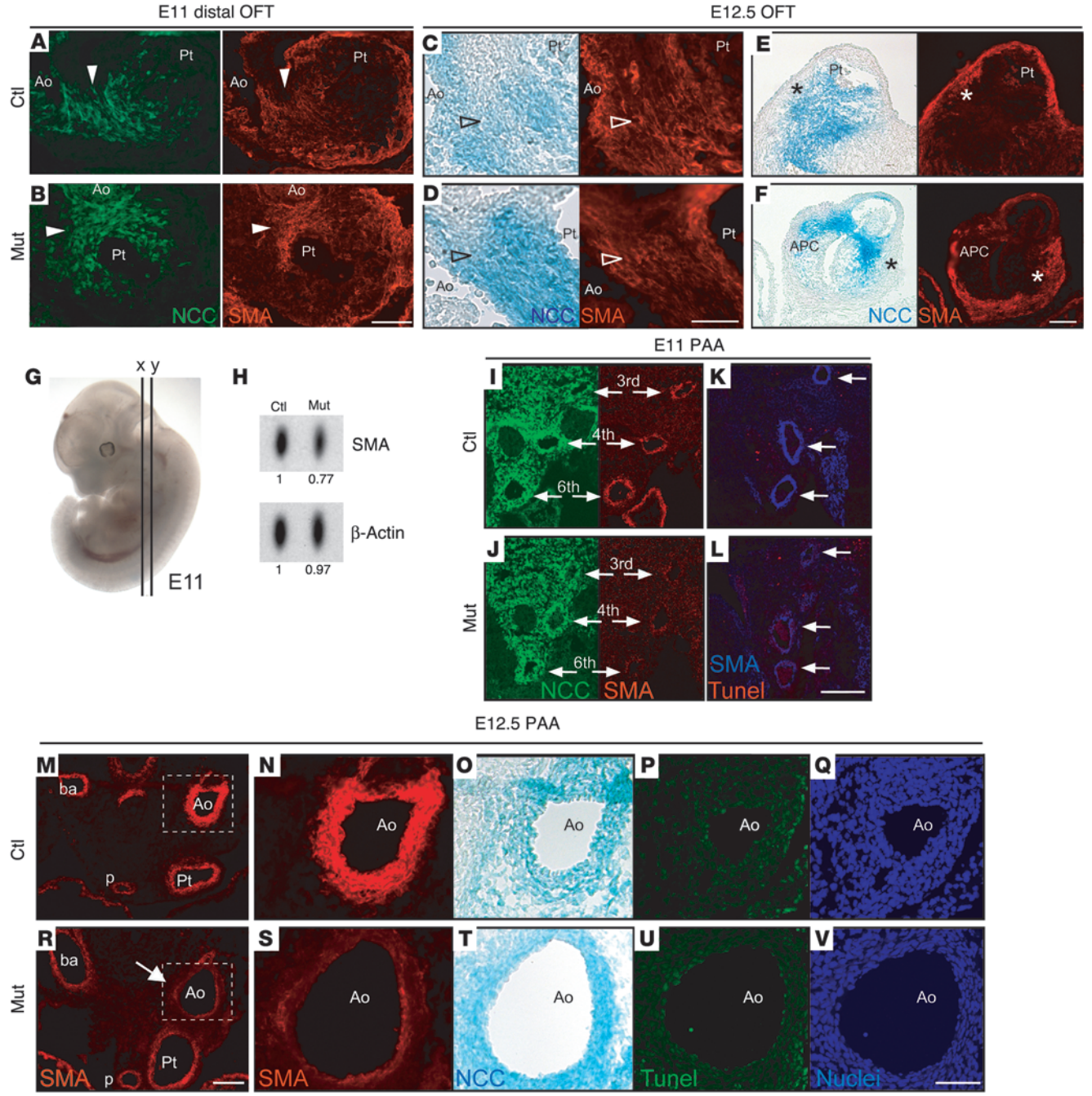

Figure 3

NCC differentiation in the cardiac outflow tract and aortic arch arteries of conditional *Fak* mutant embryos. (**A**–**F**) Frontal sections of outflow tracts (OFT) stained for GFP and SMA. (**A** and **B**) At E11, NCCs expressing GFP are able to differentiate into smooth muscle in mutant embryos and control littermates (arrowheads). (**C** and **D**) At E12.5, NCCs (blue) differentiate into smooth muscle cells in the aorticopulmonary septum (arrowheads), even in mutants with abnormal aorticopulmonary communication. (**E** and **F**) Anterior sections from same embryos as in **C** and **D**, showing that myocardialization of the outflow tract in mutants is not altered (asterisks). At this stage, SMA stains for both smooth muscle and myocardium. (**G**) E11 embryo showing planes of sections for **A** and **B** (x) and **I**–**L** (y). (**H**) Western blot of E11 branchial arches (n = 3 embryos pooled), showing decreased SMA levels in mutants compared with control littermates. (**I**–**V**) Frontal sections through the pharyngeal arch arteries (PAA) stained for GFP, SMA, TUNEL, and DAPI. (**I** and **J**) At E11, NCCs colonize the third, fourth, and sixth pharyngeal arch arteries (arrows) in mutant and control littermates. (**K** and **L**) Reduction of SMA staining in mutant pharyngeal arch arteries (arrows) was not associated with increased NCC death. (**M**–**V**) E12.5 frontal sections showing preductal aortic arch region defective for NCC differentiation in a mutant (arrow). **N**–**Q** and **S**–**V** show higher magnification pictures from the boxed regions in **M** and **R**, respectively. **O** and **T** were stained with X-gal, and **Q** and **V** were stained with DAPI. p, pulmonary artery. Scale bars: 100 μm (**A**, **B**, **E**, **F**, **M**, and **R**); 50 μm (**I**–**L**, **N**–**Q**, and **S**–**V**); 25 μm (**C** and **D**).

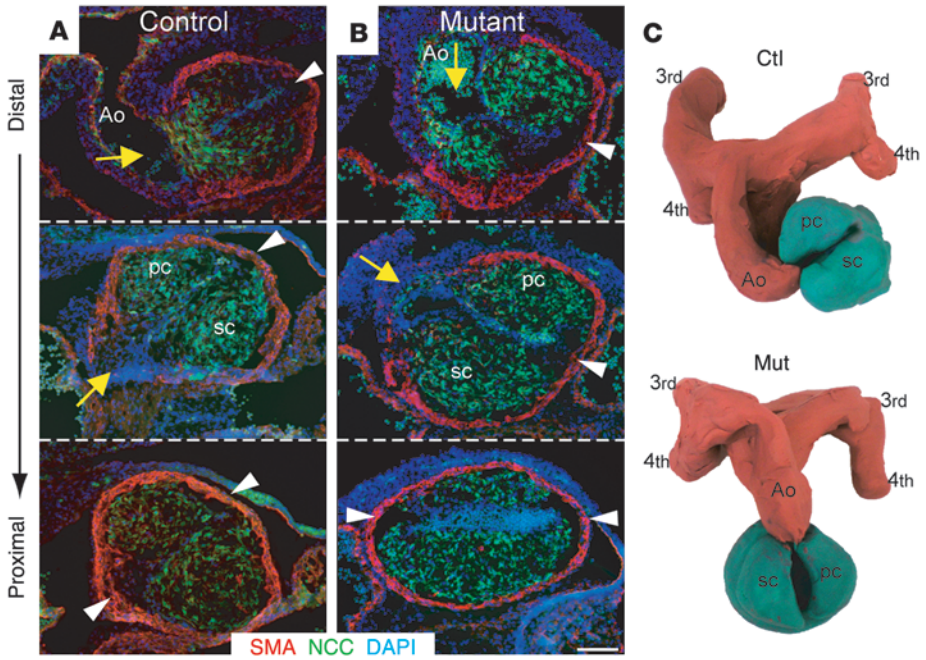

Figure 4
Impaired outflow tract rotation in conditional *Fak* mutant embryos. Distal-to-proximal frontal sections through the conotruncus of E11 control (**A**) and mutant (**B**) embryos, at the level of aortic branching from the outflow tract. Note abnormal positioning of the aorta (yellow arrows) in mutants, which is in a more dextroposed position as compared with control littermates. Arrowheads point to conotruncal cushion limits. Red shows SMA, green (GFP) shows NCCs migrating into the outflow tract, and blue stains show nuclei (DAPI). (**C**) Clay models of E11 outflow tracts based on frontal sections of *Z/EG* mutants and control littermates, showing the abnormal rotation of the outflow tract in mutant embryos. Cryostat frontal sections used for the construction of these models were 30 μm apart and triple stained with GFP (for NCC), SMA, and DAPI. Representative sections are illustrated in Supplemental Figure 5. pc, parietal cushion; sc, septal cushion; 3rd, third aortic arch. Scale bar: 100 μm.

Our observations indicate that the vascular defects observed later in development are due to inappropriate regression of aortic arch segments rather than to a failure to form these structures. It seems likely that regression results from defective smooth muscle differentiation, although these 2 defects may be mechanistically unrelated. Altogether, our data suggest that the aortic arch patterning defects observed in the conditional *Fak* mutants do not result from deficient migration or survival of NCCs in the aortic arch arteries but rather from impaired smooth muscle differentiation of NCCs.

Cardiac outflow tract defects of conditional Fak mutants. We next sought to characterize the causes of the conditional *Fak* mutant outflow tract defects. Frontal sections of E11 embryos revealed that, in contrast to controls, the distal outflow tract did not undergo counterclockwise rotation in the mutants (Figure 4). This resulted in a dextroposed aortic root and left the apposing proximal outflow tract cushions in a superoinferior position, instead of the normal side-by-side position.

Elongation of the outflow tract is required for correct cardiac looping, complete outflow tract rotation, and appropriate outflow tract alignment during aorticopulmonary septum formation (39) and requires both cardiac NCCs and the secondary (anterior) heart field. Cardiac NCCs contribute to the existing mesenchymal cushions, while cells derived from the secondary heart field contribute to the outflow tract myocardial cuff and most of the right ventricle (40, 41). Importantly, it has been shown that NCCs are required for secondary heart field cell migration to the cardiac outflow tract (42). Thus, we analyzed the secondary heart field contribution to the mutant outflow tracts, by staining them with Islet1, a secondary heart field marker (43). In E9.5 tissue sections, there was not an obvious difference in numbers of Islet1-expressing cells, between mutant and control littermates (Supplemental Figure 4A). Similarly, no difference was observed at E10.5 in secondary heart field–derived myocardium by staining with anti-MF20 (Supplemental Figure 4B). Outflow tract length was also normal in the mutant at E10.5 (Supplemental Figure 4C). Thus, we concluded that malrotation of the outflow tract in conditional *Fak* mutants is not caused by defective addition of secondary heart field cells.

We next sought to determine whether NCC-related gene expression was altered in conditional *Fak* mutants. For this, we examined the gene expression profile in the outflow tract of E11.5 mutant and control embryos using microarray analysis and subsequent quantitative RT-PCR (qPCR) validation. At this stage, outflow tract rotation deficits were already observed in mutant embryos (data deposited at National Institutes of Health Neuroscience Microarray Consortium, http://np2.ctrl.ucla.edu/np2/home.do). We focused on genes with altered expression that are known to be involved in congenital heart disease models and/or known FAK signaling pathways (data summarized in Supplemental Table 2). Some of the genes whose expression is perturbed by ablation of *Fak* are likely to affect NCC behavior directly, while others participate in the crosstalk between the NCC and other cell types necessary for proper cardiac outflow tract morphogenesis. For the genes shown on Supplemental Table 2, the ratios determined using microarray data and qPCR assays were comparable. In conditional *Fak* mutants, we identified downregulation of signaling molecules that are relevant for extracellular matrix organization (osteoglycin [*Ogn*], perlecan [*Hspg2*]), cell adhesion (L1 cell adhesion molecule [*L1cam*]), and cytoskeletal regulation (stathmin-like 3 [*Stmn3*], doublecortin [*Dcx*], phosphatidylinositol 4-phosphate 5-kinase [*Pip5k1b*]). In addition, our analysis revealed upregulation of semaphorin 3C, a signaling molecule involved in outflow tract septation and aortic arch remodeling (44). Interestingly, disruption of some of these genes, such as perlecan (45), paired related homeobox 1 (*Prrx1*) (46), and semaphorin 3C (*Sema3c*) (44), prevents normal cardiovascular development.

Abnormal NCC morphogenesis in Fak mutant outflow tracts. A detailed analysis of the NCCs in E11.0 outflow tract cushions, using phalloidin red to stain filamentous actin, showed that *Fak*-deficient NCCs do not form a normal condensed mesenchyme (Figure 5A). In control embryos, the distal ends of the parietal and septal conotruncal cush-

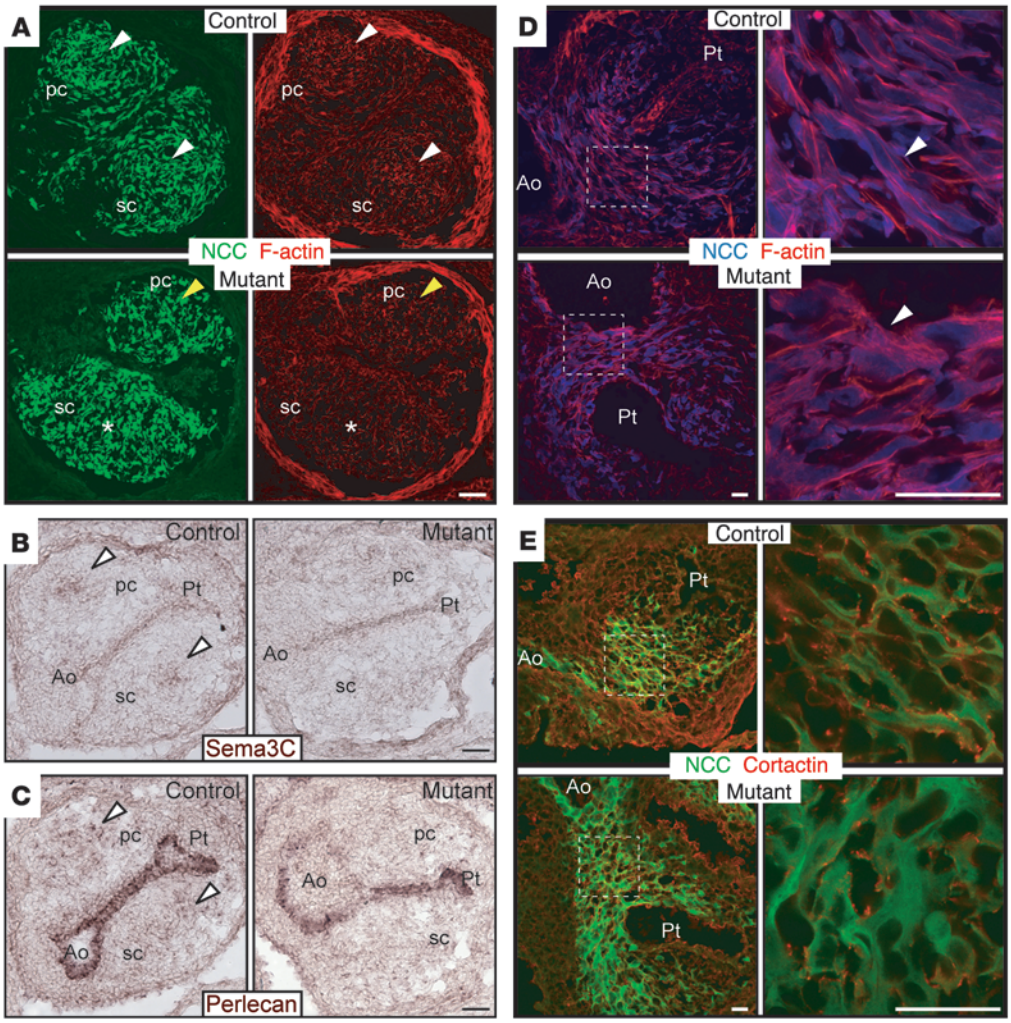

Figure 5

Abnormal NCC organization and morphology in conditional *Fak* mutant embryos. (**A**–**C**) Transverse outflow tract sections of control and mutant E11.0 embryos. (**A**) Compared with control, GFP (green, NCCs) and phalloidin staining (red) demonstrate an abnormal organization of NCCs in conotruncal cushions of mutants. Note highly condensed mesenchyme of NCCs in the center of conotruncal cushions in control littermates (white arrowheads). In mutants, in contrast, these condensed structures are not found (asterisk) or they are disorganized and mislocalized to the edges of conotruncal cushions, near the myocardial layer (yellow arrowhead). (**B** and **C**) Semaphorin 3C (Sema3C) and perlecan in situ hybridization show reduced expression in the conotruncal cushions of *Fak*-deficient E11 outflow tracts (arrowheads). (**D** and **E**) Cryostat sections of E11.0 embryos at the level of the aorticopulmonary septum. (**D**) Compared with control, *Fak*-deficient NCCs (blue) show a rounder morphology and a disorganized actin cytoskeleton, demonstrated by phalloidin staining (red). Right panels show higher magnification images from boxed areas in left panels. Note that in control NCCs, F-actin is organized in parallel fibers as opposed to *Fak*-deficient NCCs (arrowheads). (**E**) *Fak*-deficient NCCs (green) show reduced cortactin (red) localization to the cell periphery in the aorticopulmonary septum compared with control littermates. Right panels show higher magnification images from boxed areas in left panels. Scale bars: 50 μm (**A**–**C**); 30 μm (**D** and **E**).

ions contain a central rod of condensed mesenchymal cells of neural crest origin. When both ridges fuse, their central rods of condensed mesenchyme fuse also to form a central mass of SMA-positive cells. In most mutants, the central rod of condensed mesenchyme could not be detected or was misplaced. When present, the condensed mesenchyme formed by *Fak*-deficient NCCs appeared to be more scattered and disorganized than that in control littermates (Figure 5A and Supplemental Figure 6A). Subsequently, we examined the expression of some of the genes identified in the microarray and qPCR analysis, using in situ hybridization and immunohistochemical techniques. Interestingly, we found that semaphorin 3C, expressed both in the condensed NCC mesenchyme and the myocardial cuff, was indeed downregulated in the NCCs of *Fak* mutant outflow tracts (Figure 5B). Thus, its upregulation in microarray and qPCR analyses is probably due to an increased expression by the myocardial cuff. We also analyzed expression of the extracellular matrix proteins perlecan (Figure 5C) and osteoglycin (Supplemental Figure 6B). Each protein was downregulated in *Fak*-deficient NCCs of the conotruncal cushions, consistent with our RNA expression analyses. Therefore, our results indicate that *Fak* deletion results in an abnormal morphogenic program that prevents normal formation of a condensed mesenchyme by mutant NCCs.

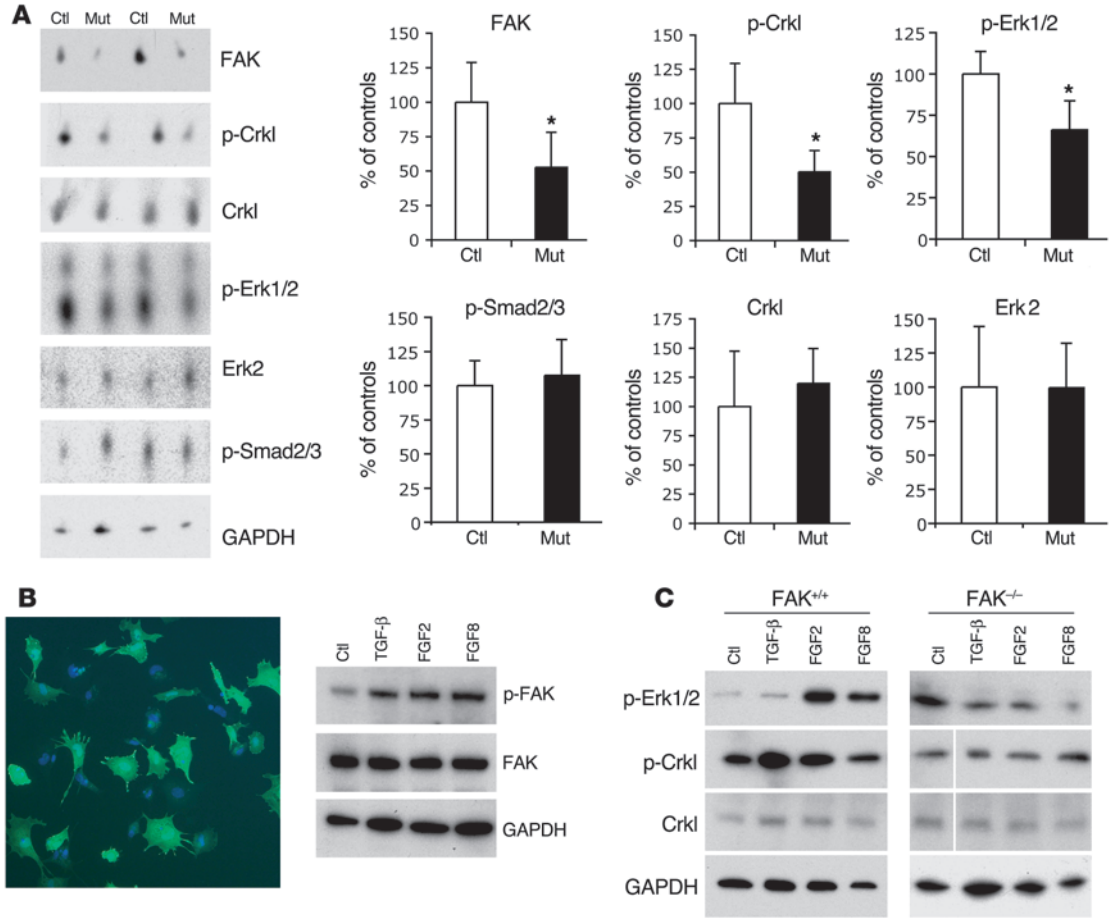

Figure 6

FAK-dependent Crkl and Erk1/2 phosphorylation in NCCs. (**A**) Decreased Crkl and Erk1/2 phosphorylation in mutant outflow tracts. Western blot analysis of control and mutant outflow tract samples showing significant decrease of FAK levels (52.74% ± 25.37%; $n = 4$), phospho-Crkl levels (p-Crkl levels, 50.24% ± 18.78%), and phopho-Erk1/2 (p-Erk1/2 levels, 66.19% ± 17.56%) in mutants compared with control littermates (100%; $n = 4$; $^*P \leq 0.05$). Total levels of Crkl, Erk2, phospho-Smad2/3 (p-Smad2/3), and GAPDH are not significantly changed. Statistical significance was determined using nonpaired, 2-tailed Student's *t* test. Data are expressed as mean ± SD. (**B**) Increased FAK phosphorylation in NCCs in vitro after addition of growth factors. Photograph illustrating an in vitro NCC culture stained with GFP-488 to show recombinant NCC cells from *Wnt1CreZ/EG* embryos and DAPI for nuclear staining (left panel). Original magnification, ×100. Western blot analysis reveals increased FAK phosphorylation in NCCs in vitro after 30 minutes of incubation with different growth factors (TGF-β, FGF2, and FGF8) compared with nontreated control cells (right panel). Three independent experiments yielded similar results. (**C**) Increased Erk1/2 and Crkl phosphorylation are observed in wild-type NCCs after addition of FGF2/FGF8 and TGF-β/FGF2, respectively. No obvious changes in Erk1/2 or Crkl phosphorylation are observed in *Fak*-deficient NCCs after growth factor addition. White lines indicate noncontiguous lanes run on the same gel.

Next, we examined the aorticopulmonary septum region (Figure 5, D and E) at E11.0 and noticed that, when present, this septum was observed in fewer serial sections and was therefore more limited in extent in conditional *Fak* mutants compared with control littermates. Although we found that NCCs migrate, survive, and appear to differentiate comparatively normally, deficient aorticopulmonary septum development can be attributed to a number of other causes. First, this process involves interactions between diverse cell types, including myocardium, endocardium, and NCCs. Also, deficient aorticopulmonary septation is related to abnormal outflow tract rotation, even in the presence of NCCs (47). Moreover, our data indicated that *Fak*-deficient NCCs were not able to form a functional condensed mesenchyme, which might be affecting proper development of the aorticopulmonary septum. More strikingly, we detected marked differences in the actin cytoskeleton of *Fak*-deficient NCCs. While control NCCs had an elongated morphology and exhibited well-formed stress fibers, oriented parallel to the longitudinal axis of each cell, *Fak*-deficient NCCs had a more rounded morphology, with more dispersed filamentous actin and fewer, thinner, less oriented stress fibers (Figure 5D). There was also reduced localization at the cell periphery of cortactin, an F-actin binding protein, in the NCCs (Figure 5E). Cortactin is involved in tyrosine kinase–, Rac1-, and Cdc42-dependent pathways that promote activation of a complex containing actin-related protein 2 (Arp2) and Arp3 that regulates protrusive-based cell motility (48). FAK is also known to regulate Rho activity through interactions with p190RhoGEF and p190RhoGAP, resulting in elevated or impaired Rho-dependent signaling, depending upon cell type (49, 50). Our results demonstrated that in the aorticopulmonary septum region, *Fak*-deficient NCCs have defective

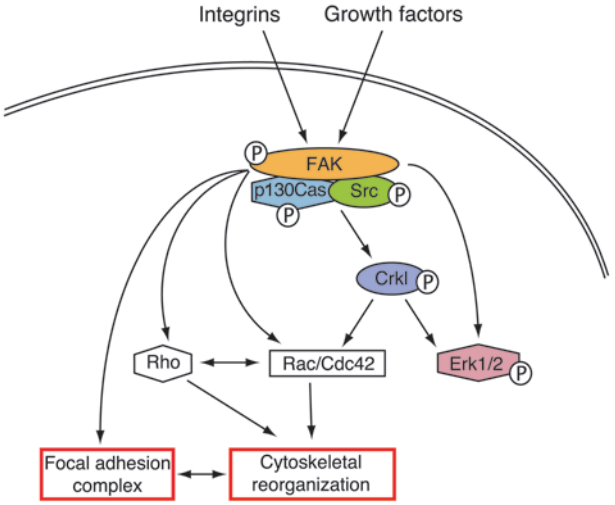

Figure 7
Model for FAK requirement in NCCs during cardiovascular development. FAK signaling is required by postmigratory NCCs for appropriate cell function. In NCCs, FAK is phosphorylated by integrin activation and growth factors, such as TGF-β and FGFs. *Fak*-deficient NCCs are unable to propagate or integrate certain integrin and growth factor signals. Specifically, during outflow tract septation, Crkl and Erk1/2 phosphorylation is impaired in *Fak*-deficient NCCs, leading to cardiac developmental defects that recapitulate DiGeorge syndrome. Deficient Crkl phosphorylation potentially affects Crkl binding ability, through its SH2 domain, to other proteins, such as paxillin and p130CAS, and translocation of Crkl to focal adhesions. Therefore, activation of Rac1 and Cdc42 is potentially affected in *Fak*-deficient NCCs, which results in reduced cortactin localization to the cell periphery, abnormal cell morphology, and cytoskeletal reorganization.

regulation of the actin cytoskeleton and abnormal NCC morphology, suggesting a potential impairment of NCC invasion during fusion of the conotruncal ridges, which could, in turn, disturb aorticopulmonary septation.

Reduced levels of phospho-Crkl and phospho-Erk1/2 in mutant outflow tracts. Ablation of the 22q11 genes *Crkl* and *Erk2* in mice generates phenotypes similar to those observed following *Fak* deletion in NCCs (5, 51). Specifically, Crkl-null mice have obvious cardiovascular and craniofacial abnormalities, with normal migration and early expansion but impaired survival of NCCs (5, 13). Moreover, inactivation of TGF-β signaling in a mouse model of congenital heart disease impairs Crkl phosphorylation in NCCs (33). Thus, we analyzed the levels of Crkl and Erk1/2 phosphorylation in E12.5 *Fak* conditional mutant and control outflow tracts (Figure 6A; $n = 4$). Western blots demonstrated that the levels of Crkl and Erk1/2 phosphorylation in mutant lysates were significantly lower than those of their control littermates (50% and 66%, respectively; $P < 0.05$), even though total Crkl and Erk2 levels were unchanged. However, levels of phospho-Smad2/3, a TGF-β reporter, were not significantly altered in mutant outflow tracts. GAPDH staining was used to verify equal protein loading. As expected, FAK was significantly downregulated in mutant outflow tracts (53%; $P < 0.05$).

Since Crkl signaling is activated through FGFs, TGF-β, and integrins (13, 33, 52), we next sought to determine whether FGFs and TGF-β also activate FAK in NCCs. For this, we isolated NCCs from the branchial arches and cultured them in vitro (Figure 6B). Purity of these cultures was assessed by *Wnt1creZ/EG* recombination, which documented that more than 75% of the cells were NCCs in origin. In these cultures, FAK phosphorylation was greatly increased after addition of TGF-β, FGF2, or FGF8. Thus, in NCCs, FAK is a downstream target of these growth factors, so TGF-β, FGF2, and FGF8 signaling is very likely to be defective in NCC derivatives in *Fak* mutants in vivo. Finally, we analyzed the effects of these growth factors on Crkl and Erk1/2 phosphorylation in NCCs in vitro (Figure 6C). Interestingly, TGF-β and FGF2 resulted in elevated phosphorylation of Crkl, while FGF2 and FGF8 increased Erk1/2 phosphorylation. These phosphorylation increases were not detected in *Fak*-deficient NCCs. Substantial FAK downregulation in mutant NCC cultures was assessed by Western blot (Supplemental Figure 7). These responses are very likely NCC specific, although we cannot rule out non–cell-autonomous effects of other cell populations present in our cultures.

Collectively, our results are consistent with the view that growth factors, such as the FGFs and TGF-β, activate through FAK Crkl and Erk1/2 phosphorylation during NCC morphogenesis and that impaired activation of this pathway is likely the underlying cause of the cardiovascular and craniofacial abnormalities found in the conditional *Fak* mutants (see Figure 7 for model).

Discussion

In this study, we have examined the phenotypes resulting from targeted deletion of *Fak* in NCCs. Conditional *Fak* mutants present craniofacial and cardiovascular malformations that lead to early postnatal lethality and resemble common genetic forms of human congenital heart disease. Mutants display cleft palate together with several cardiovascular defects, including persistent truncus arteriosus, overriding aorta, ventricular septal defect, and type B interruption of the aortic arch.

FAK functions in multiple signaling pathways, including the ones initiated by integrins, FGFs, and TGF-β (8, 10, 53). We found that TGF-β, FGF2, and FGF8 are able to induce FAK phosphorylation and FAK-mediated phosphorylation of Erk1/2 and Crkl in NCCs in vitro. Interestingly, we found that conditional *Fak* mutant mice share strikingly similar phenotypes with murine models of DiGeorge syndrome, such as mice with a 1.5-Mb deletion in the critical 22q11 region (21); ablation of *Crkl*, which maps within this region (5); or *Erk2* deletion, localized to a distal region in chromosome 22q11 (51). Disruption of Tbx1, FGF8, and TGF-β signaling also generates many features of DiGeorge syndrome (7, 22–24, 33, 38, 54). However, inactivation of Tbx1 or FGF8 results in abnormal patterning of the aortic arch arteries and defective migration or survival of NCCs, leading to conotruncal heart defects (7, 23). In contrast, the development of aortic arch defects in *Fak* mutant mice is due to failures in NCC differentiation, not migration or survival, and initial formation of aortic arch arteries seems normal. Thus, phenotypic differences do not support a close association between Tbx1 or FGF8 genetic pathways and FAK signaling in NCCs. Moreover, recent studies have provided evidence that NCCs are not direct targets of secondary heart field–derived FGF signaling (55, 56).

In this study, we show that *Fak* mutant outflow tracts have reduced Crkl and Erk1/2 phosphorylation, indicating that Crkl and Erk1/2 are FAK effectors in NCCs during outflow tract septation. This is especially interesting, since NCC-specific *Erk2* and *Crkl* mutant mice recapitulate the major features of DiGeorge syndrome. Crkl is an adaptor that functions downstream of integrin, FGF, and TGF-β receptors to recruit signaling complexes that

activate Ras and Rac (13, 33, 52). Based upon our data, we propose that FAK, Crkl, and Erk1/2 participate in a common pathway, which is involved in the NCC morphogenetic program during outflow tract development, that when perturbed results in DiGeorge syndrome–associated cardiac phenotypes (Figure 7). In the future, it will be interesting to determine whether there are genetic interactions between FAK and DiGeorge syndrome–associated genes.

Tests on murine mutants have shown that defects in multiple signaling pathways that affect cardiac NCCs prevent normal development of the aortic arch arteries and cardiac outflow tract, with individual mutants affecting NCC proliferation, survival, migration, or differentiation (57, 58). Our results indicate that NCCs lacking FAK migrated normally, which is surprising given the importance of FAK in cell motility (8). NCC migration in vivo and in vitro is primarily mediated by β_1 integrins (14, 59, 60). Integrins promote NCC motility, in part, through protein tyrosine kinase activation (61). In this regard, a recent study has shown that FAK signaling is required for $\alpha_5\beta_1$ but not $\alpha_4\beta_1$ integrin-stimulated neuroblastoma cell motility (62). Moreover, in *Fak*-null fibroblasts, expression of $\alpha_4\beta_1$ rescued cell motility defects (63). Thus, our results are consistent with prior studies, documenting a major role for $\alpha_4\beta_1$ integrin in NCC migration (59, 64, 65). As noted above, NCC-specific integrin β_1 deletion, using Ht-PA-Cre, which is not expressed before NCCs begin migration, does not result in cardiac abnormalities (17). The same paper cited unpublished observations, indicating that cardiac NCCs are perturbed when integrin β_1 is deleted at an earlier time in NCC precursors. Thus, it is not clear if β_1 integrins are required for NCC migration. These data indicate, however, that they are not essential for later cardiac NCC differentiation.

In the conditional *Fak* mutant, NCC differentiation into smooth muscle is impaired in the aortic arch arteries but appears to be comparatively normal in the cardiac outflow tract region. Thus, the essential roles of FAK in NCC derivatives must differ between these regions, probably due to the different environmental signals to which NCCs are being exposed. Alternatively, outflow tract NCCs could be expressing a different morphogenic program from the one in the aortic arch arteries that includes differentiation to smooth muscle cells through FAK-independent pathways. Interestingly, mice hemizygous for the 22q11 homologous region or with disrupted Notch or TGF-β signaling also exhibit impaired cardiac NCC differentiation into smooth muscle in the aortic arch arteries (21, 33, 66). Our study and others have shown that TGF-β can activate FAK and enhance Crkl phosphorylation (11, 33). Consequently, our data suggests that the presence of FAK is required for normal TGF-β signaling in this region through control of Crkl and possibly additional effectors.

We found that FAK is required by NCCs for correct cardiac outflow tract rotation during early cardiovascular development. Defective rotation of the outflow tract underlies the overriding aorta and persistent truncus arteriosus phenotypes found in conditional *Fak* mutants. It also appears to be related to a more rounded NCC morphology, with deficient cytoskeletal organization and reduced peripheral cell–associated cortactin in the aorticopulmonary septum. In the conotruncal cushions, we found abnormal condensed mesenchyme formation, with reduced NCC expression of perlecan, osteoglycin, and semaphorin 3C. Deficiencies in semaphorin 3C or perlecan result in congenital cardiovascular defects in mice (44, 45). Interestingly, TGF-β induces perlecan expression, which binds and modulates integrin and growth factor activities (FGF, PDGF) (67).

NCC influx is required for outflow tract rotation (39). *Splotch* (also known as *Pax3*) mutant mice have reduced NCC colonization of the cardiac outflow tract and developed several outflow tract defects, including persistent truncus arteriosus and double-outlet right ventricle, together with defective rotation of the outflow tract myocardial wall (47, 68). Conditional *Fak* mutants, however, show defective rotation despite the presence of normal NCC numbers. The mechanisms resulting in cardiac outflow tract rotation remain largely unknown, although the cytoskeleton appears essential to induce the rotational forces associated with heart looping (69). Several mouse models with an incomplete cardiac outflow tract rotation exhibit abnormal cytoskeleton organization of the outflow tract myocardium (70, 71). Also, mutation of the folate transport gene, *Folr1,* affects cytoskeletal organization in conotruncal tissues, preventing normal outflow tract development (72).

FAK signaling may modulate the NCC actin cytoskeleton through many mechanisms (8). FAK promotes focal adhesion turnover through dynamin. Also, FAK regulates Rho family GTPases through Crkl, p190RhoGEF, p190RhoGAP, and other upstream regulators. FAK regulates N-WASP, an Arp2/3 complex activator. In addition, binding of the FAK FERM domain to Arp2/3 controls protrusive lamellipodia formation and cell spreading (73). Through Rho, FAK controls cytoskeletal contractility and microtubule stability.

Cardiac outflow tract morphogenesis requires crosstalk between NCCs, secondary heart field, myocardium, mesenchymal, and endothelial cells. As part of this study, we performed an RNA profile analysis using control and *Fak* mutant E11.5 cardiac outflow tracts. Results revealed interesting candidates downregulated in the *Fak* mutant, including several microtubule regulators (Stmn3, Dcx) and a FAK-associated phospholipid kinase (Pip5k1b). Interestingly, both Stmn3 and Pip5k1b are known to interact with Rac GTPase signaling and may help explain the altered NCC morphology and actin cytoskeleton observed in mutant NCCs.

In conclusion, our results demonstrate that the presence of FAK in NCCs is required for appropriate cardiac outflow tract morphogenesis and aortic arch remodeling. Given the multiple targets of FAK, future studies will be necessary to clarify the roles of various FAK-regulated signaling pathways in cardiac development. In addition, future analyses of NCC-specific knockout mice that survive to adulthood should reveal functions of FAK in other NCC derivatives.

Methods

Mouse lines. The $Fak^{flox/flox}$ (27), *R26R* (31), *Z/EG* (32), and *Wnt1cre* (28) mice were maintained on mixed genetic backgrounds. $Wnt1creFak^{flox/flox}$ mutants were compared with control littermates ($Fak^{+/flox}$, $Fak^{flox/flox}$, $Wnt1creFak^{+/flox}$). Genotyping for Fak and cre alleles was determined by PCR as previously described (27, 28). The stage of embryo development was determined with the day of plug being E0.5. All animals were handed in accordance with protocols approved by the UCSF Animal Care and Use Committee.

Reagents. Antibodies were obtained from the following sources: FAK polyclonal Ab (pAb) (A17; catalog no. sc-557), Crkl pAb (C20; catalog no. sc319), and Osteoglycin pAb (K14; catalog no. sc-47277) (Santa Cruz Biotechnology Inc.); SMA mAb (clone 1A4; A5228) (Sigma-Aldrich); Islet-1 mAb (39.4D5 and 40.2D6) and MF20 mAb (Developmental Studies Hybridoma Bank); phospho-histone H3 (pAb) (Upstate); phospho-FAK pAb (catalog no. 44-624G) (BioSource International); phospho-Crkl pAb (catalog no. 3181) and phospho-Erk1/2 pAb (catalog no. 9101) (Cell Signaling Technology); phospho-Smad2/3 pAb (catalog no. AB3849), Erk2

mAb (catalog no. 05-157), and GAPDH mAb (catalog no. MAB374) (Millipore). Filamentous actin was visualized using rhodamine phalloidin, and GFP-expressing NCCs were visualized using Alexa Fluor 488–conjugated anti-GFP Ab (Molecular Probes). Cell death was determined with the In Situ Cell Death Detection Kit, TMR red (Roche Applied Science). Cell nuclei were labeled with DAPI (Sigma-Aldrich).

Histology. Embryos or dissected hearts were fixed in 4% paraformaldehyde and dehydrated and embedded in paraffin wax. Sections were stained in H&E. Embryos were stained for β-galactosidase activity resulting from Cre-mediated recombination of the *Rosa26lacZ* reporter allele, using standard protocols. Fast red was used as a nuclear counterstain. Embryonic and postnatal vasculatures were visualized by intracardiac Microfil blue liquid compound injection (Flow Tech). E18.5 crania were stained with Alcian Blue and Alizarin Red to visualize bone and cartilage, using a standard protocol.

Immunohistochemistry and in situ hybridization. Embryos were fixed in 4% paraformaldehyde and embedded in OCT. For 1 hour, 12-μm cryostat sections were preincubated with 2% normal goat serum, 5% bovine serum albumin, and 0.5% Triton X-100 in PBS. Slides were incubated overnight at 4°C with primary antibodies and then washed and incubated with Alexa Fluor 488–, CY3-, or CY5-conjugated secondary antibodies (1:200; Molecular Probes). Alternatively, sections were incubated with biotinylated secondary antibodies (1:200; Vector Laboratories), VECTASTAIN ABC Kit (Vector Laboratories), and 0.05% diaminobenzidine/0.0003% H_2O_2. Primary antibodies were used at the following concentrations: SMA mAb (1:500); GFP-488 (1:500); FAK (1:100); phospho-histone H3 (1:50); MF20 (1:100); Islet-1 (1:100); osteoglycin (1:100). Analysis of gene expression using in situ hybridization with digoxigenin-labeled RNA probes was performed according to standard protocols. RNA probes were provided by J. Rubenstein (UCSF), S. Evans (UCSD), and A. Kolodkin (Johns Hopkins University School of Medicine, Baltimore, Maryland, USA).

Gene expression analyses, microarray analysis, and qPCR. RNA was extracted from the outflow tract region of E11.5 conditional *Fak* mutants and littermate controls with Absolutely RNA microprep Kit (Stratagene). RNAs from 3 embryos from each genotype were pooled to average genetic and experimental variations. cDNA reverse transcription, amplification, labeling, and hybridization to Affymetrix GeneChip 430 2.0 arrays was performed by the National Institutes of Health Neuroscience Microarray Consortium. Candidate genes were then analyzed by qPCR, as previously described (74). Briefly, cDNA was synthesized using random hexamers and SuperScript III Reverse Transcriptase (Invitrogen), following the manufacturer's instructions. Primer design was done using PrimerExpress software (Applied Biosystems; see Supplemental Table 3). FAK and osteoglycin assays were purchased from Applied Biosystems. qPCR was carried out in an ABI PRISM 7300 Sequence Detection System (Applied Biosystems). Target genes were normalized by using *GAPDH* and *B2m* as internal control genes. Fold change of gene expression was calculated in mutant versus control samples.

Western blot analysis. Tissues were dissected and lysed in modified RIPA buffer (10 mM Triton X-100, 0.5% sodium deoxycholate, 0.1% SDS, 10 mM Tris, pH 7.5, 100 mM NaCl, 1 mM EDTA, 1 mM EGTA, 10% glycerol, 1 mM $NaVO_4$, 1 mM NaF, and 1x Complete Mini Protease Cocktail [Roche Applied Science]). Using a method to enhance sensitivity based on a previous study (75), 1 μg protein was loaded onto each lane. Culture NCCs were lysed directly in 50 mM Tris, 2% SDS, 0.1% bromophenol blue, 10% glycerol, 5% β-mercaptoethanol, pH 6.8. Protein lysates were separated on 4%–15% gradient SDS-PAGE gels (Bio-Rad). Proteins were transferred onto PVDF membranes (Immobilon-P; Millipore), blocked with 5% nonfat milk/1% goat serum, and incubated with antibodies to FAK (1:200), phospho-FAK (1:1,000), Crkl (1:100), phospho-Crkl (1:1,000), Erk2 (1:1,000), phospho-Erk1/2 (1:1,000), phospho-Smad2/3 (1:1,000), or GAPDH (1:700) overnight at 4°C. Primary antibodies were detected with anti-rabbit or anti-mouse HRP-conjugated secondary antibodies (10 ng/ml) (Pierce), which were visualized using SuperSignal West Dura Chemiluminescent Substrate and Femto Trial Kit (Pierce). Protein band densitometry was carried out using ImageJ version 1.34s software (http://rsbweb.nih.gov/ij/).

NCC cultures. Preparation of NCCs from branchial arches was performed as previously described (76, 77). Briefly, first and second branchial arches from E10.5 embryos were dissected and incubated in 0.125% trypsin and 1 mM EDTA at 37°C for 10 minutes. After trypsin neutralization, cells were collected by centrifugation and seeded in 6-well plates in DMEM/F12 (1:1; GIBCO-BRL), containing 10% FBS (GIBCO-BRL), leukemia inhibitor factor (LIF) (10^6 U/l; Chemicon International), 0.1 M nonessential amino acids (GIBCO-BRL) plus penicillin and streptomycin (100 μg/ml). After a 30-minute incubation, unattached cells were discarded and fresh medium was added to the wells. Cultures were maintained in a humidified atmosphere of 5% CO_2 at 37°C. NCCs were seeded in 12-well plates at 150,000 cells/well and, after 24 hours, were preincubated with DMEM/F12 for 1 hour before addition of growth factors at 20 ng/ml (TGF-β [Collaborative Research Inc.], FGF2 [Chiron Corporation], and FGF8 [R&D Systems]). Cells were incubated at 37°C for 30 minutes, then washed twice with ice-cold PBS, and lysed directly with SDS-PAGE loading buffer.

Statistics. Statistical comparisons were made by 2-tailed Student's *t*-test. Data are expressed as mean ± SD.

Acknowledgments

This work was supported by the National Institutes of Health grant 1 R01 NS19090 (to L.F. Reichardt) and a postdoctoral fellowship from Gobierno Vasco, Vitoria, Spain (to A. Vallejo-Illarramendi). We thank Deepak Srivastava, Brian Black, and members of the Reichardt laboratory for comments on the manuscript and helpful discussions; the John Rubenstein laboratory for reagents and technical assistance; and Sylvia Evans and Alexander Kolodkin for RNA probes.

Received for publication December 1, 2008, and accepted in revised form May 6, 2009.

Address correspondence to: Ainara Vallejo-Illarramendi or Louis F. Reichardt, Department of Physiology, UCSF, Rock Hall Room 284A, 1550 4th Street, San Francisco, California 94158-2611, USA. Phone: (415) 476-3976; Fax: (415) 476-2098; E-mail: ainaravallejo@yahoo.es (A. Vallejo-Illarramendi); Louis.Reichardt@ucsf.edu (L.F. Reichardt).

1. Hiruma, T., Nakajima, Y., and Nakamura, H. 2002. Development of pharyngeal arch arteries in early mouse embryo. *J. Anat.* **201**:15–29.
2. Hutson, M.R., and Kirby, M.L. 2003. Neural crest and cardiovascular development: a 20-year perspective. *Birth Defects Res. C Embryo Today.* **69**:2–13.
3. Creazzo, T.L., Godt, R.E., Leatherbury, L., Conway, S.J., and Kirby, M.L. 1998. Role of cardiac neural crest cells in cardiovascular development. *Annu. Rev. Physiol.* **60**:267–286.
4. Kirby, M.L., Gale, T.F., and Stewart, D.E. 1983. Neural crest cells contribute to normal aorticopulmonary septation. *Science.* **220**:1059–1061.
5. Guris, D.L., Fantes, J., Tara, D., Druker, B.J., and Imamoto, A. 2001. Mice lacking the homologue of the human 22q11.2 gene CRKL phenocopy neurocristopathies of DiGeorge syndrome. *Nat. Genet.* **27**:293–298.
6. Lindsay, E.A. 2001. Chromosomal microdeletions: dissecting del22q11 syndrome. *Nat. Rev. Genet.* **2**:858–868.
7. Vitelli, F., Morishima, M., Taddei, I., Lindsay, E.A., and Baldini, A. 2002. Tbx1 mutation causes multiple cardiovascular defects and disrupts neural crest and cranial nerve migratory pathways. *Hum. Mol. Genet.* **11**:915–922.
8. Mitra, S.K., Hanson, D.A., and Schlaepfer, D.D.

2005. Focal adhesion kinase: in command and control of cell motility. *Nat. Rev. Mol. Cell Biol.* **6**:56–68.
9. Ilic, D., et al. 1995. Reduced cell motility and enhanced focal adhesion contact formation in cells from FAK-deficient mice. *Nature.* **377**:539–544.
10. Hunger-Glaser, I., Fan, R.S., Perez-Salazar, E., and Rozengurt, E. 2004. PDGF and FGF induce focal adhesion kinase (FAK) phosphorylation at Ser-910: dissociation from Tyr-397 phosphorylation and requirement for ERK activation. *J. Cell Physiol.* **200**:213–222.
11. Thannickal, V.J., et al. 2003. Myofibroblast differentiation by transforming growth factor-beta1 is dependent on cell adhesion and integrin signaling via focal adhesion kinase. *J. Biol. Chem.* **278**:12384–12389.
12. Guris, D.L., Duester, G., Papaioannou, V.E., and Imamoto, A. 2006. Dose-dependent interaction of Tbx1 and Crkl and locally aberrant RA signaling in a model of del22q11 syndrome. *Dev. Cell.* **10**:81–92.
13. Moon, A.M., et al. 2006. Crkl deficiency disrupts Fgf8 signaling in a mouse model of 22q11 deletion syndromes. *Dev. Cell.* **10**:71–80.
14. Alfandari, D., Cousin, H., Gaultier, A., Hoffstrom, B.G., and DeSimone, D.W. 2003. Integrin alpha-5beta1 supports the migration of Xenopus cranial neural crest on fibronectin. *Dev. Biol.* **260**:449–464.
15. Strachan, L.R., and Condic, M.L. 2003. Neural crest motility and integrin regulation are distinct in cranial and trunk populations. *Dev. Biol.* **259**:288–302.
16. Thiery, J.P. 2003. Cell adhesion in development: a complex signaling network. *Curr. Opin. Genet. Dev.* **13**:365–371.
17. Pietri, T., et al. 2004. Conditional beta1-integrin gene deletion in neural crest cells causes severe developmental alterations of the peripheral nervous system. *Development.* **131**:3871–3883.
18. Liang, X., et al. 2007. Pinch1 is required for normal development of cranial and cardiac neural crest-derived structures. *Circ. Res.* **100**:527–535.
19. Maschhoff, K.L., and Baldwin, H.S. 2000. Molecular determinants of neural crest migration. *Am. J. Med. Genet.* **97**:280–288.
20. Sieber-Blum, M., and Zhang, J.M. 1997. Growth factor action in neural crest cell diversification. *J. Anat.* **191**:493–499.
21. Kochilas, L., et al. 2002. The role of neural crest during cardiac development in a mouse model of DiGeorge syndrome. *Dev. Biol.* **251**:157–166.
22. Brown, C.B., et al. 2004. Cre-mediated excision of Fgf8 in the Tbx1 expression domain reveals a critical role for Fgf8 in cardiovascular development in the mouse. *Dev. Biol.* **267**:190–202.
23. Abu-Issa, R., Smyth, G., Smoak, I., Yamamura, K., and Meyers, E.N. 2002. Fgf8 is required for pharyngeal arch and cardiovascular development in the mouse. *Development.* **129**:4613–4625.
24. Choudhary, B., et al. 2006. Cardiovascular malformations with normal smooth muscle differentiation in neural crest-specific type II TGFbeta receptor (Tgfbr2) mutant mice. *Dev. Biol.* **289**:420–429.
25. Kaartinen, V., et al. 2004. Cardiac outflow tract defects in mice lacking ALK2 in neural crest cells. *Development.* **131**:3481–3490.
26. Molin, D.G., et al. 2004. Transforming growth factor beta-SMAD2 signaling regulates aortic arch innervation and development. *Circ. Res.* **95**:1109–1117.
27. Beggs, H.E., et al. 2003. FAK deficiency in cells contributing to the basal lamina results in cortical abnormalities resembling congenital muscular dystrophies. *Neuron.* **40**:501–514.
28. Danielian, P.S., Muccino, D., Rowitch, D.H., Michael, S.K., and McMahon, A.P. 1998. Modification of gene activity in mouse embryos in utero by a tamoxifen-inducible form of Cre recombinase. *Curr. Biol.* **8**:1323–1326.
29. Trainor, P.A., and Tam, P.P. 1995. Cranial paraxial mesoderm and neural crest cells of the mouse embryo: co-distribution in the craniofacial mesenchyme but distinct segregation in branchial arches. *Development.* **121**:2569–2582.
30. Gruber, P.J., and Epstein, J.A. 2004. Development gone awry: congenital heart disease. *Circ. Res.* **94**:273–283.
31. Soriano, P. 1999. Generalized lacZ expression with the ROSA26 Cre reporter strain. *Nat. Genet.* **21**:70–71.
32. Novak, A., Guo, C., Yang, W., Nagy, A., and Lobe, C.G. 2000. Z/EG, a double reporter mouse line that expresses enhanced green fluorescent protein upon Cre-mediated excision. *Genesis.* **28**:147–155.
33. Wurdak, H., et al. 2005. Inactivation of TGFbeta signaling in neural crest stem cells leads to multiple defects reminiscent of DiGeorge syndrome. *Genes Dev.* **19**:530–535.
34. van den Hoff, M.J., et al. 1999. Myocardialization of the cardiac outflow tract. *Dev. Biol.* **212**:477–490.
35. Waller, B.R., 3rd, et al. 2000. Conotruncal anomalies in the trisomy 16 mouse: an immunohistochemical analysis with emphasis on the involvement of the neural crest. *Anat. Rec.* **260**:279–293.
36. Hakim, Z.S., et al. 2007. Conditional deletion of focal adhesion kinase leads to defects in ventricular septation and outflow tract alignment. *Mol. Cell. Biol.* **27**:5352–5364.
37. Boot, M.J., et al. 2004. Cardiac outflow tract malformations in chick embryos exposed to homocysteine. *Cardiovasc. Res.* **64**:365–373.
38. Bartram, U., et al. 2001. Double-outlet right ventricle and overriding tricuspid valve reflect disturbances of looping, myocardialization, endocardial cushion differentiation, and apoptosis in TGF-beta(2)-knockout mice. *Circulation.* **103**:2745–2752.
39. Yelbuz, T.M., et al. 2002. Shortened outflow tract leads to altered cardiac looping after neural crest ablation. *Circulation.* **106**:504–510.
40. Black, B.L. 2007. Transcriptional pathways in second heart field development. *Semin. Cell Dev. Biol.* **18**:67–76.
41. Snider, P., Olaopa, M., Firulli, A.B., and Conway, S.J. 2007. Cardiovascular development and the colonizing cardiac neural crest lineage. *ScientificWorldJournal.* **7**:1090–1113.
42. Waldo, K.L., et al. 2005. Cardiac neural crest is necessary for normal addition of the myocardium to the arterial pole from the secondary heart field. *Dev. Biol.* **281**:66–77.
43. Cohen, E.D., et al. 2007. Wnt/beta-catenin signaling promotes expansion of Isl-1-positive cardiac progenitor cells through regulation of FGF signaling. *J. Clin. Invest.* **117**:1794–1804.
44. Feiner, L., et al. 2001. Targeted disruption of semaphorin 3C leads to persistent truncus arteriosus and aortic arch interruption. *Development.* **128**:3061–3070.
45. Costell, M., et al. 2002. Hyperplastic conotruncal endocardial cushions and transposition of great arteries in perlecan-null mice. *Circ. Res.* **91**:158–164.
46. Bergwerff, M., et al. 2000. Loss of function of the Prx1 and Prx2 homeobox genes alters architecture of the great elastic arteries and ductus arteriosus. *Virchows Arch.* **436**:12–19.
47. Bajolle, F., et al. 2006. Rotation of the myocardial wall of the outflow tract is implicated in the normal positioning of the great arteries. *Circ. Res.* **98**:421–428.
48. Ammer, A.G., and Weed, S.A. 2008. Cortactin branches out: roles in regulating protrusive actin dynamics. *Cell. Motil. Cytoskeleton.* **65**:687–707.
49. Lim, Y., et al. 2008. PyK2 and FAK connections to p190Rho guanine nucleotide exchange factor regulate RhoA activity, focal adhesion formation, and cell motility. *J. Cell Biol.* **180**:187–203.
50. Schober, M., et al. 2007. Focal adhesion kinase modulates tension signaling to control actin and focal adhesion dynamics. *J. Cell Biol.* **176**:667–680.
51. Newbern, J., et al. 2008. Mouse and human phenotypes indicate a critical conserved role for ERK2 signaling in neural crest development. *Proc. Natl. Acad. Sci. U. S. A.* **105**:17115–17120.
52. Li, L., Guris, D.L., Okura, M., and Imamoto, A. 2003. Translocation of CrkL to focal adhesions mediates integrin-induced migration downstream of Src family kinases. *Mol. Cell. Biol.* **23**:2883–2892.
53. Tallquist, M.D., and Soriano, P. 2003. Cell autonomous requirement for PDGFRalpha in populations of cranial and cardiac neural crest cells. *Development.* **130**:507–518.
54. Frank, D.U., et al. 2002. An Fgf8 mouse mutant phenocopies human 22q11 deletion syndrome. *Development.* **129**:4591–4603.
55. Park, E.J., et al. 2008. An FGF autocrine loop initiated in second heart field mesoderm regulates morphogenesis at the arterial pole of the heart. *Development.* **135**:3599–3610.
56. Zhang, J., et al. 2008. Frs2alpha-deficiency in cardiac progenitors disrupts a subset of FGF signals required for outflow tract morphogenesis. *Development.* **135**:3611–3622.
57. High, F., and Epstein, J.A. 2007. Signalling pathways regulating cardiac neural crest migration and differentiation. *Novartis Found. Symp.* **283**:152–161; discussion 161–164, 238–241.
58. Stoller, J.Z., and Epstein, J.A. 2005. Cardiac neural crest. *Semin. Cell Dev. Biol.* **16**:704–715.
59. Kil, S.H., Krull, C.E., Cann, G., Clegg, D., and Bronner-Fraser, M. 1998. The alpha4 subunit of integrin is important for neural crest cell migration. *Dev. Biol.* **202**:29–42.
60. Kil, S.H., Lallier, T., and Bronner-Fraser, M. 1996. Inhibition of cranial neural crest adhesion in vitro and migration in vivo using integrin antisense oligonucleotides. *Dev. Biol.* **179**:91–101.
61. Brennan, H., Smith, S., and Stoker, A. 1999. Phosphotyrosine signalling as a regulator of neural crest cell adhesion and motility. *Cell. Motil. Cytoskeleton.* **42**:101–113.
62. Wu, L., et al. 2008. Distinct FAK-Src activation events promote alpha5beta1 and alpha4beta1 integrin-stimulated neuroblastoma cell motility. *Oncogene.* **27**:1439–1448.
63. Hsia, D.A., et al. 2005. Integrin alpha4beta1 promotes focal adhesion kinase-independent cell motility via alpha4 cytoplasmic domain-specific activation of c-Src. *Mol. Cell. Biol.* **25**:9700–9712.
64. Beauvais-Jouneau, A., et al. 1997. Direct role of the carboxy-terminal cell-binding domain of fibronectin in neural crest cell motility. *Exp. Cell Res.* **233**:1–10.
65. Testaz, S., Delannet, M., and Duband, J. 1999. Adhesion and migration of avian neural crest cells on fibronectin require the cooperating activities of multiple integrins of the (beta)1 and (beta)3 families. *J. Cell Sci.* **112**:4715–4728.
66. High, F.A., et al. 2007. An essential role for Notch in neural crest during cardiovascular development and smooth muscle differentiation. *J. Clin. Invest.* **117**:353–363.
67. Bix, G., and Iozzo, R.V. 2008. Novel interactions of perlecan: unraveling perlecan's role in angiogenesis. *Microsc. Res. Tech.* **71**:339–348.
68. Conway, S.J., Henderson, D.J., Kirby, M.L., Anderson, R.H., and Copp, A.J. 1997. Development of a lethal congenital heart defect in the splotch (Pax3) mutant mouse. *Cardiovasc. Res.* **36**:163–173.
69. Linask, K.K., and Vanauker, M. 2007. A role for the cytoskeleton in heart looping. *ScientificWorldJournal.* **7**:280–298.
70. Phillips, H.M., Murdoch, J.N., Chaudhry, B., Copp, A.J., and Henderson, D.J. 2005. Vangl2 acts via RhoA signaling to regulate polarized cell movements during development of the proximal outflow tract. *Circ. Res.* **96**:292–299.
71. Zhou, W., et al. 2007. Modulation of morphogenesis by noncanonical Wnt signaling requires ATF/

CREB family-mediated transcriptional activation of TGFbeta2. *Nat. Genet.* **39**:1225–1234.
72. Zhu, H., et al. 2007. Differentially expressed genes in embryonic cardiac tissues of mice lacking Folr1 gene activity. *BMC Dev. Biol.* **7**:128.
73. Serrels, B., et al. 2007. Focal adhesion kinase controls actin assembly via a FERM-mediated interaction with the Arp2/3 complex. *Nat. Cell Biol.* **9**:1046–1056.
74. Vallejo-Illarramendi, A., Domercq, M., and Matute, C. 2005. A novel alternative splicing form of excitatory amino acid transporter 1 is a negative regulator of glutamate uptake. *J. Neurochem.* **95**:341–348.
75. Swank, M.W., Kumar, V., Zhao, J., and Wu, G.Y. 2006. A novel method of loading samples onto mini-gels for SDS-PAGE: increased sensitivity and Western blots using sub-microgram quantities of protein. *J. Neurosci. Methods.* **158**:224–233.
76. Deng, M.J., et al. 2004. Multilineage differentiation of ectomesenchymal cells isolated from the first branchial arch. *Tissue Eng.* **10**:1597–1606.
77. Lin, Y., et al. 2006. Proliferation and pluripotency potential of ectomesenchymal cells derived from first branchial arch. *Cell Prolif.* **39**:79–92.